3898 *Biochemistry* **2010,** *49,* 3898–3907
DOI: 10.1021/bi100056v

BIOCHEMISTRY
including biophysical chemistry & molecular biology
Article

Interfacial Properties of Apolipoprotein B292−593 (B6.4−13) and B611−782 (B13−17). Insights into the Structure of the Lipovitellin Homology Region in Apolipoprotein B[†]

Libo Wang, Zhenghui Gordon Jiang, C. James McKnight, and Donald M. Small*

Department of Physiology and Biophysics, Boston University School of Medicine, Boston, Massachusetts 02118

Received January 13, 2010; Revised Manuscript Received March 29, 2010

ABSTRACT: The N-terminal sequence of apolipoprotein B (apoB) is critical in triacylglycerol-rich lipoprotein assembly. The first 17% of apoB (B17) is thought to consist of three domains: B5.9, a β-barrel, B6.4−13, a series of 17 α-helices, and B13−17, a putative β-sheet. B5.9 does not bind to lipid, while B6.4−13 and B13−17 contain hydrophobic interfaces that can interact with lipids. To understand how B6.4−13 and B13−17 might interact with triacylglycerol during lipoprotein assembly, the interfacial properties of both peptides were studied at the triolein/water interface. Both B6.4−13 and B13−17 are surface active. Once bound, the peptides can be neither exchanged nor pushed off the interface. Some residues of the peptides can be ejected from the interface upon compression but readsorb on expansion. B13−17 binds to the interface more strongly. The maximum pressure the peptide can withstand without being partially ejected (Π_{max}) is 19.2 mN/m for B13−17 compared to 16.7 mN/m for B6.4−13. B13−17 is purely elastic at the interface, while B6.4−13 forms a viscous-elastic film. When they are spread at an air/water interface, the limiting area and the collapse pressures are 16.6 Å^2/amino acid and 31 mN/m for B6.4−13 and 17.8 Å^2/amino acid and 35 mN/m for B13−17, respectively. The α-helical B6.4−13 contains some hydrophobic helices that stay bound and prevent the peptide from leaving the surface. The β-sheets of B13−17 bind irreversibly to the surface. We suggest that during lipoprotein assembly, the N-terminal apoB starts recruiting lipid as early as B6.4, but additional sequences are essential for formation of a lipid pocket that can stabilize lipoprotein emulsion particles for secretion.

Apolipoprotein B-containing lipoproteins, including chylomicrons, very-low-density lipoproteins (VLDLs),[1] intermediate-density lipoproteins (IDL), and low-density lipoproteins (LDL), are the major carriers of triacylglycerol (TAG) and cholesterol in human plasma (*1*, *2*). apoB is the major nonexchangeable component of these apoB-containing lipoproteins. It exists in two forms in humans, the full-length apoB (B100) and the truncated N-terminal 48% of apoB (B48). B100 in liver and B48 in intestine recruit and assemble phospholipids, TAGs, and cholesterol to form nascent TAG-rich emulsion particles that are secreted into plasma in the form of VLDL and chylomicrons, respectively. In plasma, these lipoproteins are remodeled by the action of lipid exchange proteins and various lipases. Chylomicrons are converted to chylomicron remnants, and VLDL is converted to IDL and then LDL. These lipoproteins are taken up mainly in the liver via receptor-regulated endocytotic pathways. Elevated levels of apoB-containing lipoprotein particles are a major risk factor for atherosclerosis (*1*, *2*). However, adequate apoB is required for transportation of TAG and cholesterol in the bloodstream to peripheral tissues for energy usage, fat storage, cell membrane synthesis and maintenance, and steroid hormone production. apoB binds irreversibly to lipid and has an extensive conformational flexibility to fulfill the need to cover and stabilize the lipoprotein particles of varied sizes and different lipid and apolipoprotein compositions (*3*−*7*).

B100 is a huge glycoprotein consisting of 4536 amino acid residues with a molecular mass of 550 kDa. Electron micrographs of apoB solubilized in sodium deoxycholate micelles show a 650 Å long flexible beaded ribbon of varied width (*8*). In electron microscopy reconstructions, LDL particles appear to be quasi spherical particles approximately 220−240 Å in diameter with a high-density protein ring surrounding a low-density lipid core (*9*). The N-terminus appears to form a domain projecting from the surface. It is generally accepted that apoB can be divided into five superdomains: NH2-$\beta\alpha$1-β1-α2-β2-α3-COOH (*10*−*12*). The α2 and α3 domains and β1 and β2 domains comprise predominantly amphipathic α-helix (AαH) and amphipathic β-strand (AβS) structures, respectively, and are believed to be the major lipid-associating motifs of apoB (*10*−*15*). On the other hand, the $\beta\alpha$1 superdomain encompassing the N-terminus to B22 (residues 1−1000) contains both α-helix and β-sheet structure and is predicted to have a globular, multidomain structure (*10*). The assembly of nascent lipoprotein particles happens cotranslationally in the ER, i.e., when the N-terminus of apoB is folded with lipids to form a precursor lipoprotein, the C-terminus is still being synthesized by the ribosome (*16*−*18*). Moreover, microsomal triglyceride transfer protein (MTP), an essential ER-localized

[†]This work is supported in part by National Heart, Lung and Blood Institute Grant 2P01 HL26335-21.

*To whom correspondence should be addressed: Department of Physiology and Biophysics, Boston University School of Medicine, 700 Albany St., W-302, Boston, MA 02118. Telephone: (617) 638-4001. Fax: (617) 638-4041. E-mail: dmsmall@bu.edu.

[1]Abbreviations: apoB, apolipoprotein B; VLDL, very-low-density lipoprotein; IDL, intermediate-density lipoprotein; LDL, low-density lipoprotein; TAG, triacylglycerol; B100, full-length apoB; B48, N-terminal 48% of apoB; AαH, amphipathic α-helix; AβS, amphipathic β-strand; MTP, microsomal triglyceride transfer protein; DMPC, dimyristoylphosphatidylcholine; LV, lipovitellin; TO/W, triolein/water; A/W, air/water.

 Published on Web 03/30/2010 © 2010 American Chemical Society

cofactor, is required in lipoprotein assembly (*19*, *20*). Two MTP binding sites are present in the N-terminal βα1 domain, residues 1−300 and 430−570 (*21*, *22*). Further evidence shows that loss of the disulfide bonds in the N-terminus abolishes secretion from the cell (*23*−*25*). Thus, the N-terminal sequence is responsible for initiation of lipid recruitment, and proper folding of the βα1 domain is critical in lipoprotein assembly and secretion.

Dashti et al. (*26*) showed that in McA-RH7777 cells B22 (the first 1000 amino acids) is necessary for the formation of a nascent lipoprotein particle containing both TAG and phospholipids. Alternatively, Shellness et al. (*27*) used apoB/MTP-transfected COS cells to show that B19.5 (the first 884 amino acids) is capable of forming some lipoproteins. B17 (the first 782 amino acids) secreted from MTP-deficient C127 cells contains a very small amount of surface lipid (*28*). However, B17 binds to dimyristoylphosphatidylcholine (DMPC) (*27*, *28*), phospholipid/TAG emulsions (*29*), and TAG droplets (*30*) in vitro. B19 and B20.1 also bind to TAG droplets (*31*). Thus, the N-terminal 22% of apoB contains lipid-associating domains and has the required elements to form a primordial lipoprotein particle, and under certain conditions, shorter constructs are also adequate (*27*).

Sequence alignment and analysis show that the βα1 domain is homologous in sequence and amphipathic motifs with lipovitellin (LV) (*21*, *32*−*36*). LV is an ancient lipid transport and storage protein that delivers lipids into oocytes and appears to be a putative ancestor protein of apoB (*36*, *37*). The crystal structure of lamprey LV has been determined at 2.8 Å resolution (*32*). It is comprised of a globular β-barrel domain (also called the N-sheet domain), an α-helical domain, and a lipid binding pocket which is lined up with two antiparallel β-sheet domains (the C-sheet and A-sheet). On the basis of the structure of LV, homologous models for the N-terminal domain of apoB have been built. Mann et al. (*21*) modeled the first 587 amino acids of apoB and showed that the homologous β-barrel domain and the central helical domain are conserved. Segrest et al. (*33*) modeled the whole βα1 domain and showed that it contains domains homologous to the β-barrel, α-helix, and two β-sheet domains and proposed a lipid pocket model for the initiation of lipoprotein particle assembly.

Limited proteolysis results show that the β-barrel, α-helix, and C-sheet domains are three independently folded domains in apoB containing secondary structures consistent with the B20.5 model (Figure 1) (*35*, *38*). Lipid binding experiments show that B5.9 does not bind phospholipids, while B6.4−13 and B13−17 have hydrophobic interfaces that interact with DMPC to form discoidal particles (*38*). Other fragments of apoB such as B6.4−9, B13−15, B6.4−15, and B6.4−17 bind phospholipids as well. Thus, B17 contains lipid binding structures that could bind lipids during or immediately after translocation to initiate lipoprotein assembly.

Oil-drop tensiometry has been used to study the lipid binding of apolipoproteins and consensus peptides at a TAG/water interface (*13*, *30*, *31*, *39*−*44*). It assesses the surface behaviors in terms of surface adsorption, desorption, readsorption, and elastic properties to yield information about lipid−protein interactions. In a previous study, Mitsche et al. (*44*) studied the surface behavior of B6.4−17 which contains both the α-helical (B6.4−13) and β-sheet domains (B13−17) of apoB. B6.4−17 binds to a TAG/water interface and cannot be completely ejected once bound. However, part of the peptide is pushed off the surface if compressed above 16.7 mN/m (Π_{max}) and very rapidly snaps back on upon re-expansion. The authors suggested that the eight or nine N-terminal helices (B6.4−9) are the

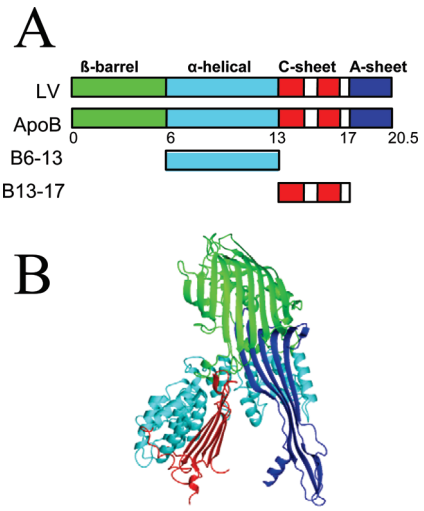

FIGURE 1: Homology model of B20.5. (A) Comparison of domain structures of lipovitellin (LV) and B20.5. Only the N-terminal 20.5% of apoB is colored by proposed domains: green for the β-barrel domain, cyan for the α-helical domain, red for the C-sheet, dark blue for the A-sheet, and white for missing regions in the structure of LV. (B) Ribbon representation of the B20.5 model colored by domain as in panel A.

structures being pushed off above 16.7 mN/m while B13−17 remains bound even at high pressures. Thus, this peptide exhibits properties of both α- and β-structure and retains some globular structure at the hydrophobic interface. In this work, we used a similar approach to study the helical (B6.4−13) and sheet (B13−17) domains individually to test the lipid associating ability of these domains and determine the mechanism of lipid−protein interaction.

EXPERIMENTAL PROCEDURES

Materials. Two apoB fragments encompassing residues 292−593 (B6.4−13) and 611−782 (B13−17) were expressed from pET24a vectors (Novagen) in BL21 DE3 *Escherichia coli* cells and purified as described previously (*35*). Both peptides contain a six-His tag at the carboxyl terminus. Before interfacial tension studies, B6.4−13 was desalted in 10 mM sodium phosphate/100 mM sodium chloride buffer at pH 7.4 using a PD-10 desalting column (GE Biosciences, Pittsburgh, PA), and B13−17 was extensively dialyzed against 5 mM sodium phosphate buffer at pH 7.4. Freshly made B6.4−13 and B13−17 were divided into small aliquots, rapidly frozen in liquid nitrogen, and stored at −80 °C. Each peptide aliquot was thawed right before the experiment and discarded afterward. The concentrations of peptide stocks were determined by the Lowry protein assay (*45*).

Triolein (>99% pure) was purchased from NU-CHEK PREP, INC. (Elysian, MN), and its interfacial tension against buffer is 32 mN/m. All other reagents are of analytical grade. KCl was heated to 600 °C for 6 h to remove all organic contaminants before it was used (*41*).

Interfacial Tension (γ) *Measurements*. The interfacial tension of the triolein/water (TO/W) interface in the presence of different amounts of B6.4−13 or B13−17 in the aqueous phase was measured with an I. T. CONCEPT (Longessaigne, France) Tracker oil-drop tensiometer (*46*). Peptide stocks were added to the aqueous phase (2 mM phosphate buffer at pH 7.4) to yield different peptide concentrations from 1.9×10^{-8} to 2×10^{-7} M for B6.4−13 and from 7.5×10^{-8} to 3×10^{-7} M for B13−17. A

16 μL triolein drop was formed in the aqueous phase, and the interfacial tension (γ) was recorded continuously until it approached an equilibrium level. The surface pressure, Π, is the γ of the interface without a peptide (γ_{TO} = 32 mN/m) minus the γ of the interface with a peptide (γ_{pep}); i.e., $\Pi = \gamma_{TO} - \gamma_{pep}$. All experiments were conducted at 25 ± 0.1 °C in a thermostated system.

Instantaneous Compression and Expansion of the Interface. To study the desorption and readsorption behavior of bound peptides at the interface, near-instant compression and expansion experiments were conducted. Once γ approached an equilibrium level, the oil drop (16 μL) was compressed by a sudden decrease in the volume at different ratios (from 6 to 75%). The compressed volume was held for several minutes and then was increased back to the original volume and held for several minutes until γ re-equilibrated. The sudden decrease in drop volume (V) instantaneously decreases the drop surface area (A) and results in a sudden compression causing γ to drop abruptly to a certain level, γ_0. The surface pressure generated is $\Pi_0 = \gamma_{TO} - \gamma_0$, where γ_{TO} is the surface tension of pure triolein (32 mN/m). If bound peptide or regions of the peptide desorb from the surface, γ will increase toward an equilibrium value (desorption curve). If the peptide does not desorb, then γ will remain essentially constant at the same low level. On re-expansion, free peptide molecules in the aqueous phase or regions of the peptide being ejected from the surface can readsorb onto the newly formed surface, and γ will fall back to the equilibrium (readsorption curve). If the readsorption curve ($d\gamma/dt$) is the same as the original adsorption curve, then we conclude that the entire peptide is ejected from the surface. If, however, $d\gamma/dt$ is much faster, then only part of the peptide is pushed off at compression and snaps back very rapidly when the area is re-expanded (*40*).

Determination of the Π_{max} Values. To estimate the maximum pressure (Π_{max}) that a peptide can withstand without being fully or partly ejected from the interface, a series of instantaneous compression and re-expansion experiments using different changes in surface area over a wide range of peptide concentrations were conducted. The tension change, $\Delta\gamma$, over the compression period was plotted against the instant pressure generated right after the compression, Π_0. Then the data were fitted to a straight line. The $\Delta\gamma = 0$ intercept gives the Π at which the peptide molecules show no net adsorption or desorption, which is Π_{max} (*40*, *41*).

Oscillation of the Interface and Elasticity Analysis. Oscillations were conducted after the equilibrium γ (γ_e) was reached. The drop volume (16 μL) was sinusoidally oscillated at varied amplitudes (6−50% change in volume) and periods (8−128 s). The changes in area (A) and γ were followed as the volume (V) oscillated. In the elasticity analysis, the interfacial elasticity modulus, ε ($\varepsilon = d\gamma/d \ln A$), the phase angle, ϕ, between the compression and the expansion, the elasticity real part, ε', and the elasticity imaginary part, ε'', were obtained ($\varepsilon' = |\varepsilon| \cos \phi$, and $\varepsilon'' = |\varepsilon| \sin \phi$) (*47*, *48*).

Buffer Exchange Procedure. With the surface tension at equilibrium (γ_e), the aqueous phase buffer (6 mL) containing the peptide was exchanged for buffer without peptide using the protocol described previously (*39*, *44*). The aqueous phase was continuously removed from the aqueous surface, and the new buffer was continuously infused near the bottom of the stirred cuvette. At least ~150 mL of buffer was exchanged. If peptide desorbs into the aqueous phase during or after buffer exchange, the surface concentration of the peptide will fall and γ will rise.

The instant compression and expansion experiments and the oscillation experiments were also conducted after buffer exchange and compared with those conducted before buffer exchange. Three basically different behaviors are possible. First, if bound peptide is pushed off the surface during compression, then on re-expansion γ will rise to a higher level and stay there since there is virtually no peptide available in the aqueous phase to adsorb back onto the newly formed surface. Second, if only part of the peptide molecule is pushed off the surface on compression, then on re-expansion γ will fall rapidly back to the same equilibrium level since the ejected part of peptide readsorbs back on the surface. Finally, compression may cause a conformational change in the peptide which sequesters part of it from the surface, and the sequestered part only very slowly rebinds to the surface after re-expansion to lower γ back to the equilibrium level (*39*).

Langmuir Balance Studies at the Air/Water (A/W) Interface. A solution of each peptide in 30% (w/v) 2-propanol and 2 mM phosphate buffer (pH 7.4) was spread slowly (~50 μL/min) on a clean surface of 3.5 M KCl and 10 mM phosphate buffer (pH 7.4) on a KSV 5000 mini trough of a Langmuir/Pockles (Helsinki, Finland) surface balance at 25 °C, according to the techniques of Phillips and Krebs (*49*). Then the surface was compressed at a rate of 5 mN m^{-1} min^{-1}, and the $\Pi-A$ curves for the peptide monolayer were obtained. To check the reversibility of the $\Pi-A$ isotherms, the peptide monolayer was compressed to a certain Π and then re-expanded to a Π lower than 1 mN/m at a rate of 5 mN m^{-1} min^{-1}, and the compression and expansion curves were compared. We detected the state of the peptide monolayer (liquid, condensed viscous, or solid phase) by putting talc powder on the surface, directing a fine jet of air, and directly observing the motion of talc particles (*50*, *51*). In the liquid state, the talc particles move rapidly and freely; in the condensed viscous state, they move slowly, and in the solid state, they are nearly stationary.

RESULTS

Both B6.4−13 and B13−17 Are Surface Active and Bind to the TO/W Interface. The equilibrium interfacial tension of the TO/W interface was measured with a different amount of peptides present in the aqueous phase. Panels A and B of Figure 2 are examples of interfacial tension−time curves of B6.4−13 and B13−17. Both peptides are surface active and lower the surface tension (γ) of the TO/W interface (32 mN/m) to reach an equilibrium level. The equilibrium γ is dependent on the peptide concentration in the aqueous phase. In general, the higher the peptide concentration, the lower the equilibrium γ and the less time it takes to reach the equilibrium. The γ of the TO/W interface (32 mN/m) is lowered to 14.1 mN/m with 1.5×10^{-7} M B6.4−13 in the aqueous phase and 12.6 mN/m with B13−17 at the same concentration. Thus, at similar concentrations, B13−17 decreases γ 1.5 mN/m more than B6.4−13, indicating that B13−17 has a higher affinity for the TO/W interface.

B6.4−13 Only Partially Desorbs from the TO/W Interface on Compression and Cannot Be Washed Off the Interface. Figure 3A shows an example of tension and area changes during the sudden compression and expansion of the interface for B6.4−13 before and after buffer exchange. The concentration of B6.4−13 in the aqueous phase is 1.9×10^{-7} M before buffer exchange, and the original volume of the triolein drop is 16 μL. As the figure shows, after γ approaches an

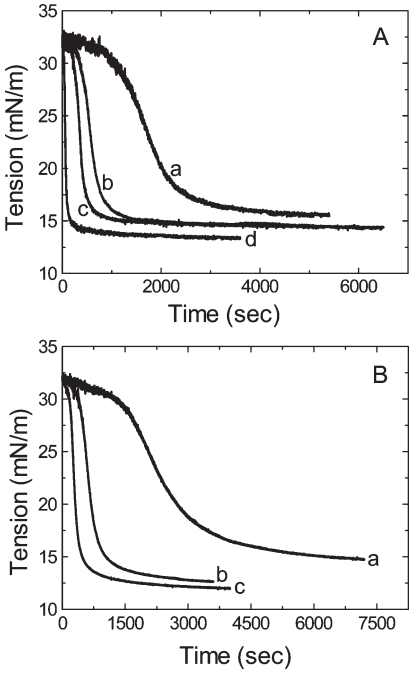

FIGURE 2: Examples of the interfacial tension (γ) vs time curves for B6.4−13 (A) and B13−17 (B) at the TO/W interface. A 16 μL triolein drop was formed in 2 mM phosphate buffer (pH 7.4) with different amounts of peptides. (A) The concentration of B6.4−13 in the aqueous phase was (a) 2×10^{-8}, (b) 3.8×10^{-8}, (c) 1.5×10^{-7}, and (d) 2.0×10^{-7} M. (B) The concentration of B13−17 in the aqueous phase was (a) 7.5×10^{-8}, (b) 1.5×10^{-7}, and (c) 3.0×10^{-7} M. All the measurements were taken at 25 ± 0.1 °C.

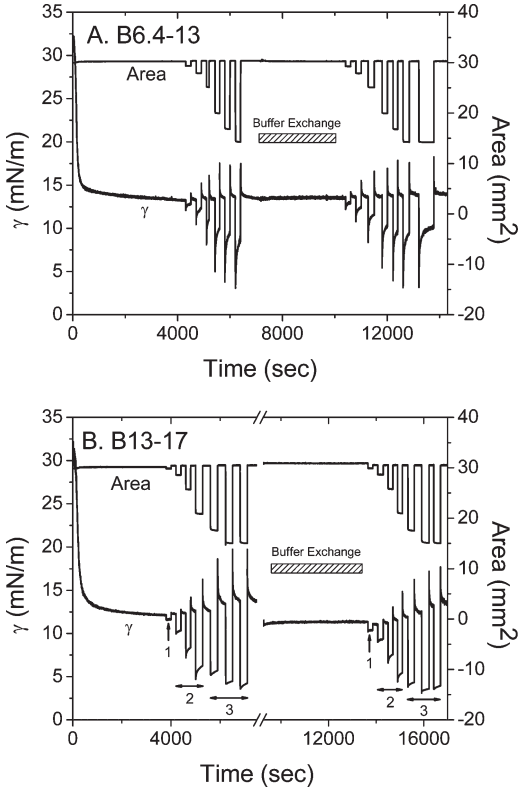

FIGURE 3: Examples of the interfacial tension (γ) and the area vs time curves for B6.4−13 (A) and B13−17 (B) at the TO/W interface and the instant compression and re-expansion measurement before and after the buffer exchange procedure. (A) The concentration of B6.4−13 in the aqueous phase was 1.9×10^{-7} M before the buffer exchange and virtually zero after the buffer exchange. A 16 μL triolein drop was formed in 2 mM phosphate buffer (pH 7.4). After γ reached an equilibrium level, the triolein drop was compressed when the volume was decreased by 1, 2, 4, 8, 10, and 12 μL (corresponding to ~3−51% changes in area) and then after several minutes re-expanded back to the original volume (16 μL) after each compression. Approximately 150 mL of buffer was exchanged during the buffer exchange procedure (shown by the bar). After the buffer exchange, the triolein drop was compressed when the volume was decreased by 1, 2, 4, 8, 10, and 12 μL (twice) and re-expanded back to the original volume (16 μL) after each compression. (B) Similar protocol applied to B13−17. The concentration of B13−17 in the aqueous phase was 2.1×10^{-7} M before the buffer exchange and virtually zero after the buffer exchange. After γ reached an equilibrium level, the triolein drop was compressed when the volume was decreased by 1, 2, 4, 8, 10, and 12 μL (twice) (corresponding to ~1−49% changes in area) and then after several minutes re-expanded back to the original volume (16 μL). Approximately 150 mL of buffer was exchanged during the buffer exchange procedure (shown by the bar). After the buffer exchange, the triolein drop was compressed when the volume was decreased by 1, 2, 4, 8, 10, and 12 μL (twice) and re-expanded back to the original volume (16 μL). All experiments were conducted at 25 ± 0.1 °C.

equilibrium level (~13.3 mN/m), the drop is compressed when the volume is decreased by 1, 2, 4, 8, 10, and 12 μL. The actual volume changes varied from 5 to 66%, and the corresponding area changes varied from 3 to 51%. Every instant compression makes γ fall, but then γ rapidly rises toward an equilibrium value while the compressed volume is held for several minutes. The drop is then re-expanded back to 16 μL after each compression. Each expansion makes the γ increase above γ_e initially. However, γ returns back to the equilibrium value (13.4 ± 0.1 mN/m) over time. Smaller compressions induce a smaller decrease in γ, while larger compression induces a greater decrease in γ. For example, at a compression of 1 μL, γ decreases from 13.3 to 12.1 mN/m and then increases to 12.8 mN/m; at the following expansion, γ increases to 14.1 mN/m and then relaxes back to the equilibrium value (13.3 mN/m). While at a compression of 12 μL, the tension decreases from 13.6 to 3.1 mN/m and then increases to 9.0 mN/m; at the following expansion, γ increases to 17.5 mN/m and then relaxes back to the equilibrium value (13.5 mN/m). After every compression, γ decreases first and then increases to a new equilibrium level, indicating that some material desorbs from the surface on instant compression.

The instant compression and expansion protocol is repeated after buffer exchange (Figure 3A, right) to determine whether the whole molecule or only some part of the bound B6.4−13 desorbs from the TO/W interface during compression. The buffer exchange procedure is started at 7300 s when γ is at the equilibrium level and stops at 10300 s (shown by the bar in Figure 3A). Approximately 150 mL of buffer is exchanged, and the concentration of B6.4−13 in the aqueous phase is reduced to virtually zero. During the buffer exchange, γ remains at the same equilibrium value (13.5 ± 0.1 mN/m) which indicates that bound B6.4−13 does not desorb from the interface. Then the instant compression and expansion procedure is applied to the triolein drop again (Figure 3A, right) like that before the buffer exchange (Figure 3A, left). The changes in γ upon compression and expansion are very similar to that before the buffer exchange. γ decreases to a similar level on compression, increases to a similar level, and then relaxes back to the similar equilibrium level after re-expansion. These data clearly show that only some part of the peptide is pushed off the interface by compression. If the whole peptide molecule is ejected from the interface on compression, then γ will remain high after re-expansion because there are

virtually no peptide molecules in the aqueous phase available to readsorb onto the surface.

Furthermore, the readsorption curves at each corresponding expansion, before and after the buffer exchange, are very similar, indicating that the readsorption is not dependent on the peptide concentration in the aqueous phase. The ejected part of the bound peptide readsorbed covering the newly generated surface so quickly that free peptide cannot adsorb onto the surface from the aqueous phase. These data further confirm that only part of B6.4−13 can be pushed off the surface. However, before or after the buffer exchange, upon compression, γ always equilibrates to a level lower than the value before compression, indicating that the remaining part of the peptide can stand compression and stays compressed to some extent. The fact that the area can be reduced 51% and on re-expansion the γ returns to equilibrium suggests that about half of the peptide is pushed off the surface in a form that can rapidly rebind.

B13−17 Only Partially Desorbs from the TO/W Interface on Compression and Cannot Be Washed Off the Interface. Figure 3B shows an example of tension and area changes during the instant compression and expansion of the interface for B13−17 before (2.1×10^{-7} M in the aqueous phase) and after the buffer exchange. γ changes in a very different way from that of B6.4−13. There are three kinds of changes in γ during the compression and re-expansion of the oil droplet at different ratios before the buffer exchange (Figure 3B, left), shown as 1−3 in Figure 3B. (1) With smaller compressions (e.g., 1 μL volume decrease), γ drops from the equilibrium value (12.2 mN/m) to 11.6 mN/m. γ remains constant when the compressed volume is held. Upon re-expansion, γ increases to 12.4 mN/m and quickly equilibrates back to the original value of 12.2 mN/m. No desorption is observed. This indicates that no B13−17 is pushed off the surface and bound B13−17 is simply compressed at the surface. (2) With intermediate compressions (e.g., 2, 4, or 8 μL volume decrease), γ decreases much further and quickly increases (0.5−1.5 mN/m) when the compressed volumes are held. At each following re-expansion, γ increases to a level higher than the original equilibrium value of 12.2 mN/m and then relaxes back toward the equilibrium. Thus, at these intermediate compressions, part of the peptide (~25%) is pushed off the interface but snaps back very quickly upon re-expansion. (3) At larger compressions (e.g., 10 and 12 μL volume decrease), γ falls deeper but bounces back very little. The desorption is slow compared to those with the intermediate compressions. At the following re-expansion, γ increases to a high level and decreases rapidly to levels higher than the equilibrium. We suggest that at these larger compressions, part of the peptide is pushed off the surface causing conformational changes in a fraction of the peptide that cannot respread rapidly. After re-expansion, the ejected region of the peptide needs a much longer time to rearrange its conformation to readsorb onto the surface. This results in a very slow change (hours) in γ toward the equilibrium level. Similar behavior is observed with the AβS domain B37−41 (*39*).

In contrast with those for B6.4−13, the desorption curves for B13−17 with compressions of >1 μL have an only slightly smaller increase in γ while the compressed volume is held. For instance, at the 8 μL compression (~30% change in the area), γ decreases from the equilibrium value to 4.9 mN/m and increases to only 6.2 mN/m; that is a 1.3 mN/m tension increase and is very small compared to the tension increase with an 8 μL expansion of B6.4−13 which is 5.0 mN/m (decreased to 5.0 mN/m and increased to 10 mN/m). This indicates that there is only a little net desorption of B13−17 with larger compressions; most of the peptide stays compressed on the surface.

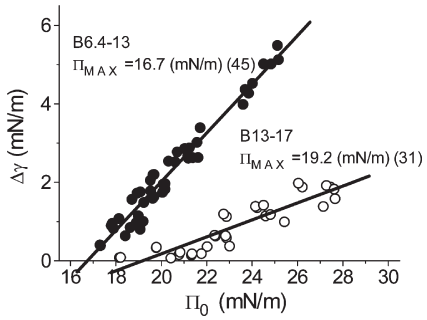

FIGURE 4: Π_{max} of B6.4−13 (●) and B13−17 (○) at the TO/W interface. The interface was instantly compressed to generate pressure Π_0; the change in the interfacial tension ($\Delta\gamma$) while the compressed volume was held for several minutes was plotted vs Π_0, and the data were fit to a straight line. The intercept of the fit lines at $\Delta\gamma = 0$ gives Π_{max}, the pressure at which peptides show no net desorption or adsorption. The data points shown are a mixture of points taken from the compression and expansion experiments before or after buffer exchange. The numbers of data points taken for each peptide are shown in parentheses.

A buffer exchange is run (shown as the bar in Figure 3B) to remove B13−17 in the aqueous phase. Similar to that of B6.4−13, γ remains the same during buffer exchange, indicating that no bound peptide desorbs from the interface. Instant compression and expansion measurements were conducted (Figure 3B, right) using the same protocol that was used before the buffer exchange (Figure 3A, left). The same three kinds of changes in the desorption and readsorption curves are observed as before the buffer exchange. Therefore, only a small part of B13−17 is pushed off the surface upon compression, and the majority of B13−17 remains on the surface. If highly compressed, the ejected region forms a conformation that is slow to respread.

Π_{max} Values for both B6.4−13 and B13−17. Instant compression followed by re-expansion measurements were taken at varied peptide concentrations to estimate the Π_{max} values for both peptides. Figure 4 shows that Π_{max} of B6.4−13 is 16.7 mN/m and Π_{max} of B13−17 is 19.2 mN/m. The data points shown are a mixture of points taken from the compression and expansion experiments before or after buffer exchange. For both peptides, the whole peptide molecule is not pushed off the surface at our study pressures, so the Π_{max} values shown here are the pressures at which parts of the peptides are ejected. A higher Π is needed to push off the ejected region of B13−17 from the interface, indicating that the ejected region of B13−17 binds to the TO/W interface more tightly than the ejected region of B6−13. In addition, $\Delta\gamma$ is always much larger for B6.4−13 than B13−17 at the same pressure, indicating that more of B6.4−13 tends to desorb from the interface than B13−17. As a matter of fact, both B6.4−13 and B13−17 can stand a very high surface pressure, e.g., 29 mN/m (Figure 3A,B) with a large compression, e.g., 12 μL (~50% decrease in area), indicating that both peptides have structures that bind strongly to the TO/W interface.

B13−17 Is Almost Purely Elastic, while B6.4−13 Has a Viscous Component on the TO/W Interface. Equilibrium oscillations of B6.4−13 and B13−17 at different amplitudes and periods were conducted before and after buffer exchange. These compressions differ from the instantaneous compressions in that they are slow, steady, sinusoidal compressions that are performed

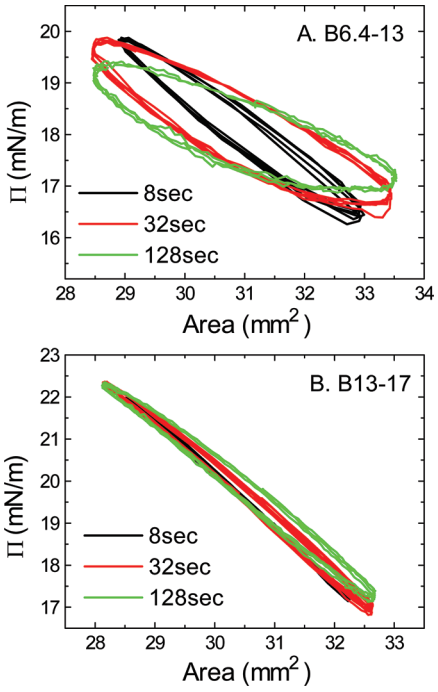

FIGURE 5: Surface pressure (Π) vs area plots for B6.4−13 (A) and B13−17 (B) at the TO/W interface derived from oscillations before the buffer exchange procedure. After the equilibrium tension (γ_e) was reached, a 16 μL triolein drop was oscillated at 16 ± 2 μL and different periods from 8 to 128 s. (A) The concentration of B6.4−13 in the aqueous phase was 1.5×10^{-7} M. (B) The concentration of B13−17 in the aqueous phase was 1.5×10^{-7} M. All experiments were conducted at 25 ± 0.1 °C.

at a set of rates. Two sets of surface pressure−area (Π−*A*) curves for B6.4−13 and B13−17 (all at 1.5×10^{-7} M in the aqueous phase) derived from the oscillations before the buffer exchange are shown in Figure 5A,B. The Π−*A* curves for B6.4−13 show significant hysteresis between compression and expansion. The corresponding phase angles, ϕ, are relatively larger, up to 30° (data not shown), indicating a visco-elastic surface. On the other hand, the Π−*A* curves for B13−17 show little hysteresis, and the phase angles are relatively small, $<10°$ (data not shown), indicating a pure elastic surface. There is very little desorption and readsorption of B13−17 during these oscillations. This is further evidence that only a small region of B13−17 desorbs and readsorbs. We conducted a series of studies on the elasticity for both peptides over a wide range of peptide concentrations, oscillation amplitudes, and oscillation periods (data not shown). The average ϕ value over all experimental conditions for B6.4−13 is 16.6 ± 7.7° and for B13−17 is 4.5 ± 3.8°, indicating that B6.4−13 forms a visco-elastic surface at the TO/W interface while B13−17 is mainly elastic. Between the two peptides, B13−17 has a higher modulus (38 ± 7.3 mN/m) than B6.4−13 (25.6 ± 6.5 mN/m). The elasticity modulus is the increase in the surface tension for a small increase in the area of a surface element ($\varepsilon = d\gamma/d \ln A$) and is the mathematical description of the surface's tendency to be deformed elastically (i.e., non-permanently) when a force is applied to it. A higher elasticity modulus indicates a more rigid molecule. This is consistent with the larger phase angles for B6.4−13 relative to B13−17. In other words, B13−17 is more rigid and less compressible than B6.4−13.

Examples of the elasticity modulus, ε, from the oscillations before and after buffer exchange are compared for both peptides

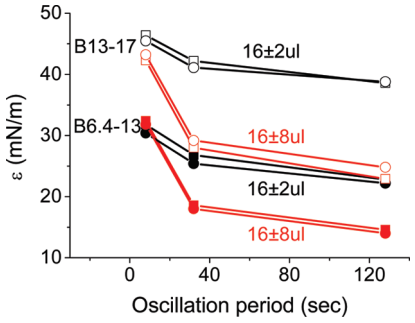

FIGURE 6: Comparison of the changes in the elasticity modulus (ε) as a function of the oscillation period of B6.4−13 and B13−17 at the TO/W interface derived from the oscillations before and after the buffer exchange procedure. The peptide concentration in the aqueous phase before buffer exchange was 2.0×10^{-7} M for B6.4−13 or 2.1×10^{-7} M for B13−17. After buffer exchange, both peptides were absent from the aqueous phase. Filled symbols are for B6.4−13, and empty symbols are for B13−17. Squares are for pre-exchange, and circles are for postexchange. Black symbols are for 16 ± 2 μL oscillations, and red symbols are for 16 ± 8 μL oscillations.

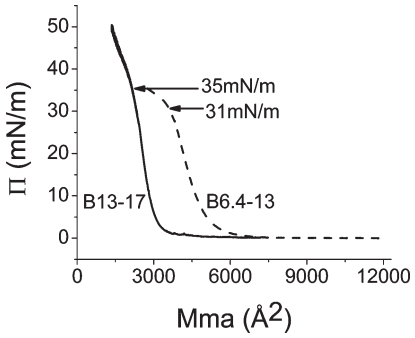

FIGURE 7: Pressure−area (Π−*A*) isotherm for B6.4−13 and B13−17 at an A/W interface. B6.4−13 (12 μg) or B13−17 (11.25 μg) in a 30% (w/v) 2-propanol/phosphate buffer mixture (pH 7.4) was spread on a 3.5 M KCl/10 mM phosphate (pH 7.4) subphase at 25 °C. The monolayer was compressed at 5 mN m^{-1} min^{-1} to produce the Π−*A* isotherm. The lift-off area is 16.6 Å^2/amino acid for B6.4−13 and 17.8 Å^2/amino acid for B13−17, while the collapse pressure is 31 mN/m (12.2 Å^2/amino acid) for B6.4−13 and 35 mN/m (13.3 Å^2/amino acid) for B13−17. Mma is equal to mean molecular area.

in Figure 6. Similar results are present either before or after the buffer exchange at the same peptide, same amplitude, and same period. One-way ANOVA analysis at the 0.05 level shows that ε, ϕ, and ε' of corresponding oscillations are not significantly different before and after buffer exchange (data not shown). This indicates that there is no whole molecule desorption from the interface or readsorption onto the interface.

Monolayers of B6.4−13 and B13−17 at the A/W Interface. Figure 7 shows the pressure−area (Π−*A*) isotherms for B6.4−13 and B13−17. The limiting area for B6.4−13 is 16.6 Å^2/amino acid, and the B6.4−13 monolayer collapses at 31 mN/m with an area of 12.2 Å^2/amino acid. The limiting area for B13−17 is 17.8 Å^2/amino acid, and the B13−17 monolayer collapses at 35 mN/m with an area of 13.3 Å^2/amino acid. Both B6.4−13 and B13−17 can be reversibly compressed and expanded at pressures below the collapse pressure (31 and 35 mN/m), respectively (data not shown). By observing the movement of the talc powder on the surface, we found that the B13−17 monolayer starts to solidify right after the lift up (Π > 2 mN/m) which is typical for a β-sheet structure (*39*). In contrast, the B6.4−13 monolayer does not solidify until Π is greater than 10 mN/m and becomes solid when

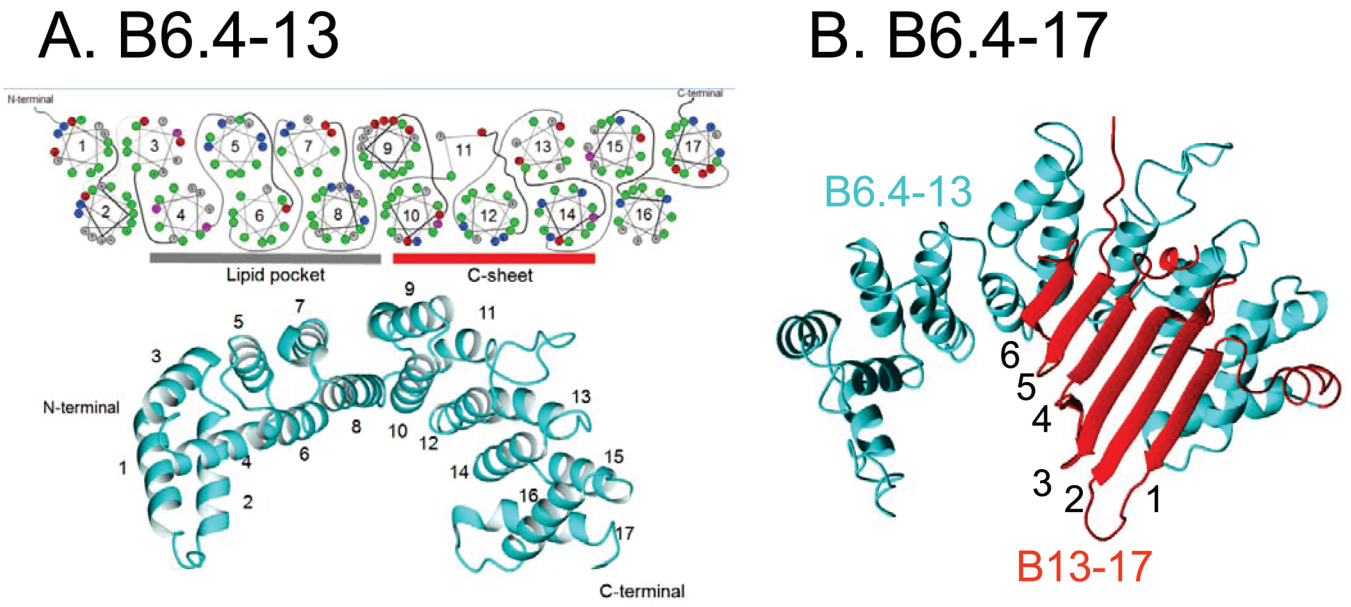

FIGURE 8: (A) B6.4−13 structural model derived from lipovitellin homology by Jiang et al. (*35*). In this model, B6.4−13 is an α-helical domain with 17 amphipathic helices forming two layers (bottom panel). The helical wheel diagram of the 17 amphipathic α-helices is shown in the top panel. Green denotes hydrophobic, gray neutral, blue positively charged, and red negatively charged residues. There is a hydrophobic core with a hydrophobic surface created by helices 4, 6, and 8 and a positively charged surface on helices 10, 12, and 14 that stabilize the negatively charged face of β-sheet domain B13−17 (C-sheet, red). The gray bar underneath the Edmondson wheels of helices 4, 6, and 8 marked "lipid pocket" indicates that helices 4−8 may form a lipid binding pocket, while the red bar underneath the Edmondson wheels of helices 10, 12, and 14 marked "C-sheet" indicates that helices 10−14 may interact with the C-sheet. The surface area of B6.4−17 at the A/W interface is 16.6 Å^2/amino acid, indicating the 17 α-helices must all lie flat on the surface. We suggest that they also lie flat on the TO/W interface. The very hydrophobic helix 6 is most likely buried in the oil phase, preventing the peptide from being pushed off the interface. (B) B6.4−17 structural model derived from lipovitellin homology by Jiang et al. (*35*), in which B13−17 (red) interacts with B6.4−13 (cyan). B13−17 is a β-sheet domain that consists of a six-stranded β-sheet with an unmodeled region between strands 4 and 5. The surface area of isolated B13−17 at the A/W interface (17.8 Å^2/amino acid) is consistent with all the amino acids interacting with the surface. We suggest that the six β-strands would lie flat at the TO/W interface at low and high pressures. The missing region between strands 4 and 5 could be the region that desorbs from the interface upon compression.

Π reaches 20 mN/m. The average area per residue for proteins adsorbed flat on a surface is 15−25 Å^2/amino acid, so both peptides are likely flat at the A/W interface.

DISCUSSION

When proteins or peptides come to hydrophobic interfaces like oil/water or air/water interfaces, different structures behave differently. When some water-soluble globular proteins adsorb to the hydrophobic interface, since they hide most of their hydrophobic residues in the core of the molecule, they undergo major conformational changes after binding and denature to gradually decrease the interfacial tension (*47*, *52*). On the other hand, apolipoproteins are specifically evolved for lipid binding with the characteristic secondary structures of AαH and AβS (*10*−*14*). When approaching a hydrophobic interface, they do not denature; instead, they rapidly adsorb and retain the secondary structures.

AαH and AβS structures exhibit characteristic interfacial properties at the TO/W interface in terms of the adsorption, the desorption and readsorption, the elasticity, and the compressibility. Both AαH and AβS structures are surface active, adsorb onto the surface, and lower the surface tension rapidly (*13*, *15*, *40*, *43*). AβS structures exhibit strong irreversible binding to the TO/W interface (*13*, *39*). They can be compressed to a very high surface pressure (∼28−29 mN/m) and stay compressed without leaving the surface. Bound AβS structures exhibit purely elastic properties with very small phase angles at the surface when the surface area changes by < 15% (*13*). When applied to an A/W interface on a monolayer trough, AβS structures quickly interact with each other when compressed to a low pressure and form a solid monolayer, suggesting a large extended β-sheet structure at very low pressures (1−2 mN/m) (*39*). This large β-sheet can be compressed and expanded reversibly up to its collapse pressure (usually ≥35 mN/m) (ref *39* and unpublished data). AαH structures show reversible binding to the TO/W surface. In general, they desorb from the surface when the surface is compressed above 13−19 mN/m (*15*, *40*, *42*) and readsorb quickly when the surface is re-expanded. This reversible on and off behavior of AαH was proposed in a review by Segrest et al. (*10*). Some AαH structures with lower surface affinity, like the N-terminal domain of apoA-I (residues 1−44), can partially desorb from the surface without compression when the peptide is exchanged out of the aqueous phase (ref *43* and unpublished data). AαH exhibits purely elastic properties only at smaller changes in the surface area and at fast rates; otherwise, it is viscoelastic at the surface (*15*, *40*, *42*). When applied to an A/W interface, an AαH structure does not become a solid monolayer until the pressure reaches well above 10 mN/m. As observed for AβS, an AαH monolayer can also be reversibly compressed and expanded as long as the pressure remains below the collapse pressure.

According to the LV homology model of B17, B6.4−13 and B13−17 are distinct domains containing α- and β-structures with amphipathic features (*35*, *38*) (Figure 8). Our study shows that B6.4−13 binds to the TO/W interface (Figure 2A) but, unlike most AαH structures, cannot be completely pushed off the TO/W interface (Figure 3A). B6.4−13 does exhibit typical partial desorption and readsorption curves of AαH structures,

Table 1: Comparison of the Surface Properties of B6.4−13, B13−17, and B6.4−17 (*44*) at TO/W and A/W Interfaces[a]

	at the TO/W interface							at the A/W interface		
peptide	γ_{eq} (mN/m) at c (M)	Π_{max} (mN/m)	ε (mN/m), $\Delta V < 25\%$	ϕ (deg)	ε' (mN/m)	exchanged off	pushed off	limiting A (Å^2/amino acid)	collapse Π (mN/m)	A at collapse (Å^2/amino acid)
B6.4−13	14.1 (1.5×10^{-7})	16.7	25.6 ± 6.5	16.5 ± 7.7	24.6 ± 7.1	no	partly	16.6	31	12.2
B13−17	12.6 (1.5×10^{-7})	19.2	38.0 ± 7.3	4.5 ± 3.8	37.8 ± 7.4	no	partly	17.8	35	13.3
B6.4−17 (*44*)	13 (1.9×10^{-7})	16.7	32.3 ± 3.9	10.3 ± 4.6	31.8 ± 4.2	no	partly	8.6	28 ± 1	7.3

[a]Definitions: γ_{eq}, equilibrium interfacial tension; Π_{max}, maximum pressure that peptide could withstand without being ejected from the interface; ε, visco-elastic modulus; ϕ, viscous phase angle, a phase difference between dγ and dA; ε', elastic component, the real part of the modulus; exchanged off, whether the peptide partly desorbs from the interface during the buffer exchange procedure; pushed off, whether the peptide desorbs from the interface when compressed; limiting A, extrapolation of the steep part of the $\Pi-A$ isotherm to the baseline giving a limiting area; collapse Π, surface pressure at which there is an abrupt change in the slope of the $\Pi-A$ isotherm above which the isotherm is not readily reversible; A at collapse, surface area per amino acid at which the peptide monolayer collapses.

i.e., fast desorption at compression and fast readsorption at re-expansion toward the equilibrium. This indicates that the majority of the secondary structure of this domain is AαH. This is consistent with the model prediction and the CD spectra that show nearly 60% its secondary structure is α-helix in B6.4−13 (*35*). Up to 50% of B6.4−13 desorbs from the TO/W interface at pressures above 16.7 mN/m (Figure 4). This is within the Π_{max} range for the AαH structures in exchangeable apolipoproteins (13−19 mN/m) and is consistent with the Π_{max} value of B6.4−17 (16.7 mN/m) (*44*). Thus, when B6.4−17 is compressed at the interface, regions in the B6.4−13 domain are pushed off at lower pressures than B13−17. The B13−17 domain has a higher lipid binding affinity with a Π_{max} of 19.2 mN/m (Figure 4), but most of the peptide remains bound, is elastic, and cannot desorb. B6.4−13 has visco-elastic properties at the TO/W interface like other AαH structures in the exchangeable apolipoproteins as well. At an A/W interface, the limiting area for the B6.4−13 monolayer is 16.6 Å^2/residue and the collapse pressure is 31 mN/m, indicating that the peptide is lying flat on the surface (Figure 7).

That B6.4−13 cannot be pushed off the interface is slightly surprising because all other AαH structures (apoA-I, apoA-I fragments, and the consensus peptides) we have studied can be pushed off the interface by compression (*15*, *40*, *42*). We note that some of the α-helix structures in the B6.4−13 domain are not those classic type A or type Y AαH structures found in exchangeable apolipoproteins or in the α2 or α3 domains of apoB (Figure 8). Some of the α-helices are very hydrophobic without a clear hydrophilic face, e.g., helices 5, 6, and 8. These helices are more similar to transmembrane α-helices, but shorter. We speculate that they may fully insert into the hydrophobic lipid and then cannot be pushed off by compression. Helices 5, 6, and 8 face the lipid pocket in the B17 model (Figure 8), especially helices 6 and 8 that bind to the lipid directly in the LV structure. Some helices in the C-terminus of B6.4−13 are typical for globular proteins and have many charged residues. They do not show strong lipid binding affinity for DMPC (*38*). In the LV homology model, those charged residues interact with the charged side of the β-sheet formed by the B13−17 domain. Mitsche et al. (*44*) have studied the interfacial properties of B6.4−17 which encompasses both the α-helical domain (B6.4−13) and the β-sheet domain (B13−17) at TO/W and A/W interfaces. Only ∼60% of the expected area of B6.4−17 binds to the A/W interface. The authors suggest that the C-terminal part of the helical domain (B9−13) retains protein−protein interactions with the hydrophilic face of the β-sheet domain and thus does not contact the surface. In our study, lacking protein−protein interactions with B13−17, those C-terminal helices of B6.4−13 with charged residues might partially denature like a globular structure and irreversibly bind to the hydrophobic interface. That is another possible reason for B6.4−13 not being fully pushed off by compression.

B13−17 shows strong binding to the TO/W interface (Figure 2B). It has a very high Π_{max} value of 19.2 mN/m (Figure 4) and is almost purely elastic (Figure 5B). B13−17 cannot be washed off or pushed off the interface (Figure 3B). Only a small region of the sequence can be pushed off the interface by compression as shown by the very small increase in the surface tension after compression (Figure 3B). This is the typical desorption behavior of AβS structures (*13*, *39*) and is consistent with the model which predicts that B13−17 contains six antiparallel β-strands forming a β-sheet (Figure 8). The readsorption curves of B13−17 at intermediate compressions show a very rapid decrease to the equilibrium level (Figure 3B), and with larger compressions, the readsorption curves return to near the equilibrium values and there is no significant difference after the buffer exchange. Together, this suggests that only a small region of B13−17 is pushed off the surface and readsorbed rapidly.

We notice that with larger compressions, the readsorption curves do not decrease to the equilibrium level (different by 1−2 mN/m). We have shown similar phenomena in our study of B37−41, a large AβS structure (*39*). When B37−41 is compressed by 36% and then re-expanded, γ increases to 23.9 mN/m and then relaxes back over 40 min to 22.7 mN/m (6.5 mN/m higher than the equilibrium, i.e., 16.2 mN/m). Then after ∼12 h, the tension gradually decreased to 19.7 mN/m. We suggest that the larger compression causes some conformational changes in the ejected region that requires more time to return to equilibrium. In the LV homology model of B20.5 (Figure 1), a large loop of amino acids (656−729) between strands 4 and 5 of the β-sheet in B13−17 is missing because this part is not present in the LV structure. This region has been predicted to contain an AαH structure (*33*). A CD study shows 30.7% α-content in B13−17 (*35*). Those helical structures might make up the region that leaves the surface upon compression and readsorbs at expansion.

Thus, both B6.4−13 and B13−17 exhibit strong binding of the lipid to the TO/W interface. Both of them contain structures that irreversibly bind to lipid. B13−17 has a higher affinity and is more elastic than B6.4−13. They show typical surface behaviors of AαH and AβS structures, suggesting that the main secondary structures of the two domains are α-helix and β-sheet, respectively, which are consistent with the homologous B17 model and with the surface study of B6.4−17 (Table 1) (*35*, *38*, *44*).

There are two competing models for the initiation of apoB assembly. A lipid pocket model is proposed in which the N-terminal 1000-residue $\beta\alpha1$ domain of apoB forms a lipid pocket homologous to that of lamprey lipovitellin during translation, which contains two β-sheets connected by a central α-helical domain and a helix−turn−helix motif close to the pocket (*53*). This pocket is gradually filled with phospholipids and converted to a nascent TAG−core emulsion particle as the translation continues. While the $\beta\alpha1$ domain contains the required sequence and structural elements for the initiation of assembly, the amino acid residues between positions 931 and 1000 may be critical for the formation of a stable, bulk lipid-containing nascent lipoprotein particle (*53*). In an alternative "intercalation−desorption model", the two sides of the lipovitellin-like cavity form solvent-accessible surfaces with strong interfacial binding properties that interact with the ER membrane to sequester neutral lipids to nucleate the oil droplet and ultimately desorb from the membrane as a small neutral lipid core-containing precursor particle (*27*). The suggestions that B19.5 is secreted in a small particle with a neutral lipid core (*27*) and that B17, B19, and B20.1 bind to a TAG/W interface (*30*, *31*) are used in support of this model. Both models agree that the N-terminal domain contains the structure and required elements for lipid binding, but they differ on the mechanism and what sequence is involved in lipid binding.

Our study shows that as early as B6.4 in the N-terminal domain of apoB, the structure possesses the ability to bind to neutral lipids. Both B6.4−13 and B13−17 contain the elements that strongly bind lipids. This is consistent with the study showing that B6.4−17, B17, B19, and B20.1 all bind to the TAG interface in vitro (*30*, *31*, *44*). In vivo studies show that truncated apoB of a different size is secreted with a different lipid composition. B17 is secreted with only a small amount of phospholipid (*28*). B22 and B19.5 are thought to be the minimum size required for lipoprotein particle assembly and secretion in different cell lines (*26*, *27*). We think that the lipid recruitment may start early, but only sequences containing a more complete lipid pocket (i.e., B19.5 or B22) can stabilize the emulsion particle and be secreted. B32.5, B37, and B41 are secreted as stable lipoprotein particles containing growing core lipids (*54*). Therefore, during apoB translocation, lipid recruiting may start as early as B6.4, but future sequences as translation continues are required to produce a stable emulsion particle which can be secreted.

In summary, our interfacial studies of the two distinct domains (B6.4−13 and B13−17) in the LV homologous N-terminal domain of apoB show that both domains contain lipid-associating structures. The majority of the secondary structure of the two domains is AαH and AβS, respectively, which is consistent with the B20.5 model. The two domains show different surface behaviors at the TO/W interface, but they work together to form a hydrophobic face to bind to the TAG surface.

REFERENCES

1. Kane, J. P., and Havel, R. J. (2001) Disorders of the Biogenesis and Secretion of Lipoproteins Containing the B Apolipoproteins. In The Metabolic Bases of Inherited Disease (Scriver, C. R., Beaudet, A. L., Sly, W. S., and Valle, D., Eds.) 8th ed., Chapter 115, pp 2717−2752, McGraw-Hill, Medical Publishing Division.
2. Havel, R. J., and Kane, J. P. (2001) Introduction: Structure and Metabolism of Plasma Lipoproteins. In The Metabolic Bases of Inherited Disease (Scriver, C. R., Beaudet, A. L., Sly, W. S., and Valle, D., Eds.) 8th ed., Chapter 114, pp 2705−2716, McGraw-Hill, Medical Publishing Division.
3. Kane, J. P. (1991) Plasma lipoproteins and their receptors. *Curr. Opin. Struct. Biol. 1*, 510–515.
4. Chen, G. C., Liu, W., Duchateau, P., Allaart, J., Hamilton, R. L., Mendel, C. M., Lau, K., Hardman, D. A., Frost, P. H., and Malloy, M. J. (1994) Conformational differences in human apolipoprotein B-100 among subspecies of low density lipoproteins (LDL). Association of altered proteolytic accessibility with decreased receptor binding of LDL subspecies from hypertriglyceridemic subjects. *J. Biol. Chem. 269*, 29121–29128.
5. McNamara, J., Small, D. M., Li, Z., and Schaefer, E. J. (1996) Differences in LDL subspecies involve alterations in lipid composition and conformational changes in apolipoprotein B. *J. Lipid Res. 37*, 1924–1935.
6. Krauss, R. M., and Burke, D. J. (1982) Identification of multiple subclasses of plasma low density lipoproteins in normal humans. *J. Lipid Res. 23*, 97–104.
7. Hurt-Camejo, E., Camejo, G., Rosengren, B., Lopez, F., Wiklund, O., and Bondjers, G. (1990) Differential uptake of proteoglycan-selected subfractions of low density lipoprotein by human macrophages. *J. Lipid Res. 8*, 1387–1398.
8. Gantz, D. L., Walsh, M. T., and Small, D. M. (2000) Morphology of sodium deoxycholate-solubilized apolipoprotein B-100 using negative stain and vitreous ice electron microscopy. *J. Lipid Res. 41*, 1464–1472.
9. Spin, J. M., and Atkinson, D. (1995) Cryoelectron microscopy of low density lipoprotein in vitreous ice. *Biophys. J. 68*, 2115–2123.
10. Segrest, J. P., Jones, M. K., De Loof, H., and Dashti, N. (2001) Structure of apolipoprotein B-100 in low density lipoproteins. *J. Lipid Res. 42*, 1346–1367.
11. Nolte, R. T. (1994) Structural Analysis of the Human Apolipoproteins: An Integrated Approach Utilizing Physical and Computational Methods. Ph.D. Thesis, Boston University School of Medicine, Boston.
12. Segrest, J. P., Jones, M. K., Mishra, V. K., Anantharamaiah, G. M., and Garber, D. W. (1994) ApoB-100 has a pentapartite structure composed of three amphipathic α-helical domains alternating with two amphipathic β-strand domains. Detection by the computer program LOCATE. *Arterioscler. Thromb. 14*, 1674–1685.
13. Wang, L., and Small, D. M. (2004) Interfacial properties of amphipathic β strand consensus peptides of apolipoprotein B at oil/water interfaces. *J. Lipid Res. 45*, 1704–1715.
14. Small, D. M., and Atkinson, D. (1997) The first β sheet region of apoB(apoB21−41) is an amphipathic ribbon 50−60 Å wide and 200 Å long which initiates triglyceride binding and assembly of nascent lipoproteins. *Circulation 96*, 1.
15. Wang, L., Atkinson, D., and Small, D. M. (2003) Interfacial properties of an amphipathic α-helix consensus peptide of exchangeable apolipoproteins at air/water and oil/water interfaces. *J. Biol. Chem. 278*, 37480–37491.
16. Pease, R. J., Harrison, G. B., and Scott, J. (1991) Co-translocational insertion of apolipoprotein B into the inner leaflet of the endoplasmic reticulum. *Nature 353*, 448–450.
17. Spring, D. J., Chen-Liu, L. W., Chartterton, J. E., Elovson, J., and Schumaker, V. N. (1992) Lipoprotein assembly. Apolipoprotein B size determines lipoprotein core circumference. *J. Biol. Chem. 267*, 14839–14845.
18. Schumaker, V. N., Phillips, M. L., and Chatterton, J. E. (1994) Apolipoprotein B and low-density lipoprotein structure: Implications for biosynthesis of triglyceride-rich lipoproteins. *Adv. Protein Chem. 45*, 205–248.
19. Wetterau, J. R., Aggerbeck, L. P., Bouma, M. E., Eisenberg, C., Munck, A., Hermier, M., Schmitz, J., Gay, G., Rader, D. J., and Gregg, R. E. (1992) Absence of microsomal triglyceride transfer protein in individuals with abetalipoproteinemia. *Science 258*, 999–1001.
20. Wetterau, J. R., Gregg, R. E., Harrity, T. W., Arbeeny, C., Cap, M., Connolly, F., Chu, C. H., George, R. J., Gordon, D. A., Jamil, H., Jolibois, K. G., Kunselman, L. K., Lan, S. J., Maccagnan, T. J., Ricci, B., Yan, M., Young, D., Chen, Y., Fryszman, O. M., Logan, J. V. H., Musial, C. L., Poss, M. A., Robl, J. A., Simpkins, L. M., Slusarchyk, W. A., Sulsky, R., Taunk, P., Magnin, D. R., Tino, J. A., Lawrence, R. M., Dickson, J. K., Jr., and Biller, S. A. (1998) An MTP inhibitor that normalizes atherogenic lipoprotein levels in WHHL rabbits. *Science 282*, 751–754.
21. Mann, C. J., Anderson, T. A., Read, J., Chester, S. A., Harrison, G. B., Kochl, S., Ritchie, P. J., Bradbury, P., Hussain, F. S., Amey, J., Vanloo, B., Rosseneu, M., Infante, R., Hancock, J. M., Levitt, D. G., Banaszak, L. J., Scott, J., and Shoulders, C. C. (1999) The structure of vitellogenin provides a molecular model for the assembly and secretion of atherogenic lipoproteins. *J. Mol. Biol. 285*, 391–408.

22. Hussain, M. M., Bakillah, A., Nayak, N., and Shelness, G. S. (1998) Amino acids 430−570 in apolipoprotein B are critical for its binding to microsomal triglyceride transfer protein. *J. Biol. Chem. 273*, 25612–25615.
23. Burch, W. L., and Herscovitz, H. (2000) Disulfide bonds are required for folding and secretion of apolipoprotein B regardless of its lipidation state. *J. Biol. Chem. 275*, 16267–16274.
24. Huang, X. F., and Shelness, G. S. (1997) Identification of cysteine pairs within the amino-terminal 5% of apolipoprotein B essential for hepatic lipoprotein assembly and secretion. *J. Biol. Chem. 272*, 31872–31876.
25. Tran, K., Boren, J., Macri, J., Wang, Y., McLeod, R., Avramoglu, R. K., Adeli, K., and Yao, Z. (1998) Functional analysis of disulfide linkages clustered within the amino terminus of human apolipoprotein B. *J. Biol. Chem. 273*, 7244–7251.
26. Dashti, N., Manchekar, M., Liu, Y., Sun, Z., and Segrest, J. P. (2007) Microsomal Triglyceride Transfer Protein Activity Is Not Required for the Initiation of Apolipoprotein B-containing Lipoprotein Assembly in McA-RH7777 Cells. *J. Biol. Chem. 282*, 28597–28608.
27. Shelness, G. S., Hou, L., Ledford, A. S., Parks, J. S., and Weinberg, R. B. (2003) Identification of the Lipoprotein Initiating Domain of Apolipoprotein B. *J. Biol. Chem. 278*, 44702–44707.
28. Herscovitz, H., Hadzopoulou-Cladaras, M., Walsh, M. T., Cladaras, C., Zannis, V. I., and Small, D. M. (1991) Expression, secretion, and lipid-binding characterization of the N-terminal 17% of apolipoprotein B. *Proc. Natl. Acad. Sci. U.S.A. 88*, 7313–7317.
29. Herscovitz, H., Derksen, A., Walsh, M. T., McKnight, C. J., Gantz, D. L., Hadzopoulou-Cladaras, M., Zannis, V., Curry, C., and Small, D. M. (2001) The N-terminal 17% of apoB binds tightly and irreversibly to emulsions modeling nascent very low density lipoproteins. *J. Lipid Res. 42*, 51–59.
30. Weinberg, R. B., Cook, V. R., DeLozier, J. A., and Shelness, G. S. (2000) Dynamic interfacial properties of human apolipoproteins A-IV and B-17 at the air/water and oil/water interface. *J. Lipid Res. 41*, 1419–1427.
31. Ledford, A. S., Cook, V. A., Shelness, G. S., and Weinberg, R. B. (2009) Structural and dynamic interfacial properties of the lipoprotein initiating domain of apolipoprotein B. *J. Lipid Res. 50*, 108–115.
32. Anderson, T. A., Levitt, D. G., and Banaszak, L. J. (1998) The structural basis of lipid interactions in lipovitellin, a soluble lipoprotein. *Structure 6*, 895–909.
33. Segrest, J. P., Jones, M. K., and Dashti, N. (1999) N-terminal domain of apolipoprotein B has structural homology to lipovitellin and microsomal triglyceride transfer protein: A "lipid pocket" model for self-assembly of apoB-containing lipoprotein particles. *J. Lipid Res. 40*, 1401–1416.
34. Read, J., Anderson, T. A., Ritchie, P. J., Vanloo, B., Amey, J., Levitt, D., Rosseneu, M., Scott, J., and Shoulders, C. C. (2000) A mechanism of membrane neutral lipid acquisition by the microsomal triglyceride transfer protein. *J. Biol. Chem. 275*, 30372–30377.
35. Jiang, Z. G., Carraway, M., and McKnight, C. J. (2005) Limited proteolysis and biophysical characterization of the lipovitellin homology region in apolipoprotein B. *Biochemistry 44*, 1163–1173.
36. Baker, M. E. (1988) Is vitellogenin an ancestor of apolipoprotein B-100 of human low-density lipoprotein and humen lipoprotein lipase. *Biochem. J. 255*, 1057–1060.
37. Meininger, T., Raag, R., Roderick, S., and Banaszak, L. J. (1984) Preparation of single crystals of a yolk lipoprotein. *J. Mol. Biol. 179*, 759–764.
38. Jiang, Z. G., Gantz, D., Bullitt, E., and McKnight, C. J. (2006) Defining lipid-interacting domains in the N-terminal region of apolipoprotein B. *Biochemistry 45*, 11799–11808.
39. Wang, L., Martin, D. D., Genter, E., Wang, J., McLeod, R. S., and Small, D. M. (2009) Surface study of apoB1694−1880 shows this sequence anchors apoB to lipoproteins and makes it nonexchangeable. *J. Lipid Res. 50*, 1340–1352.
40. Wang, L., Atkinson, D., and Small, D. M. (2005) The interfacial properties of apoA-I and an amphipathic α-helix consensus peptide of exchangeable apolipoproteins at the triolein/water interface. *J. Biol. Chem. 280*, 4154–4165.
41. Wang, L., Walsh, M. T., and Small, D. M. (2006) Apolipoprotein B is conformationally flexible but anchored at a triolein/water interface: A possible model for lipoprotein surfaces. *Proc. Natl. Acad. Sci. U.S.A. 103*, 6871–6876.
42. Wang, L., Hua, N., Atkinson, D., and Small, D. M. (2007) The N-terminal (1−44) and C-terminal (198−243) peptides of apolipoprotein A-I behave differently at the triolein/water interface. *Biochemistry 46*, 12140–12151.
43. Small, D. M., Wang, L., and Mitsche, M. A. (2009) The adsorption of biological peptides and proteins at the oil/water interface. A potentially important but largely unexplored field. *J. Lipid Res. 50*, S329–S334.
44. Mitsche, M. A., Wang, L., Jiang, Z. G., McKnight, C. J., and Small, D. M. (2009) Interfacial properties of a complex multi-domain 490 amino acid peptide derived from apolipoprotein B (residues 292−782). *Langmuir 25*, 2322–2330.
45. Lowry, O. H., Rosebrough, N. J., Farr, A. L., and Randall, R. J. (1951) Protein measurement with the Folin phenol reagent. *J. Biol. Chem. 193*, 265–275.
46. Labourdenne, S., Gaudry-Rolland, N., Letellier, S., Lin, M., Cagna, A., Esposito, G., Verger, R., and Rivière, C. (1994) The oil-drop tensiometer: Potential applications for studying the kinetics of (phospho)lipase action. *Chem. Phys. Lipids 71*, 163–173.
47. Benjamins, J., and Lucassen-Reynders, E. H. (1998) Surface Dilational Rheology of Proteins Adsorbed at Air/Water and Oil/Water Interfaces. In Proteins at Liquid Interfaces (Möbius, D., and Miller, R., Ed.) pp 341−384, Elsevier, Amsterdam.
48. Benjamins, J., Cagna, A., and Lucassen-Reynders, E. H. (1996) Viscoelastic properties of triacylglycerol/water interfaces covered by proteins. *Colloids Surf. 114*, 245–254.
49. Phillips, M. C., and Krebs, K. E. (1986) Studies of apolipoproteins at the air-water interface. *Methods Enzymol. 128*, 387–403.
50. Fahey, D. A., and Small, D. M. (1986) Surface properties of 1, 2-dipalmitoyl-3-acyl-sn-glycerols. *Biochemistry 25*, 4468–4472.
51. Fahey, D. A., and Small, D. M. (1988) Phase behavior of monolayers of 1, 2-dipalmitoyl-3-acyl-sn-glycerols. *Langmuir 4*, 589–594.
52. Beverung, C. J., Radke, C. J., and Blanch, H. W. (1999) Protein adsorption at the oil/water interface: Characterization of adsorption kinetics by dynamic interfacial tension measurements. *Biophys. Chem. 81*, 59–80.
53. Richardson, P. E., Manchekar, M., Dashti, N., Jones, M. K., Beigneux, A., Young, S. G., Harvey, S. C., and Segrest, J. P. (2005) Assembly of lipoprotein particles containing apolipoprotein-B: Structural model for the nascent lipoprotein particle. *Biophys. J. 88* (4), 2789–2800.
54. Carraway, M., Herscovitz, H., Zannis, V., and Small, D. M. (2000) Specificity of lipid incorporation is determined by sequences in the N-terminal 37% of apoB. *Biochemistry 39*, 9737–9745.